# Birefringent Fourier-transform imaging spectrometer

**Andrew Robert Harvey and David William Fletcher-Holmes**

*School of Engineering and Physical Sciences, Heriot-Watt University, Riccarton, Edinburgh EH14 4AS, UK*
*a.r.Harvey@hw.ac.uk*

*http://www.ece.eps.hw.ac.uk/~arharvey*

**Abstract:** Fourier-transform imaging spectrometers offer important advantages over other spectral imaging modalities, such as, a wider free spectral range, higher spectral resolutions and, in low-photon-flux conditions, higher signal-to-noise ratios can be achieved. Unfortunately, for application in harsh environments, deployment of Fourier-transform instruments based on traditional moving-mirror interferometers is problematic due to their inherent sensitivity to vibration. We describe a new Fourier-transform imaging spectrometer, based on a scanning birefringent interferometer. This system retains the advantages of traditional Fourier transform instruments, but is inherently compact and insensitive to vibration. Furthermore, the precision requirements of the movement can be relaxed by typically two orders of magnitude in comparison to a traditional two-beam interferometer. The instrument promises to enable application of Fourier-transform imaging spectrometry to applications, such as airborne reconnaissance and industrial inspection, for the first time. Example spectral images are presented.



**OCIS codes:** (120.6200) Spectrometers and spectroscopic instrumentation; (300.6190) Spectrometers; (300.6300) Spectroscopy, Fourier transforms; (260.1440) Birefringence; (120.0280) Remote sensing

## References and Links

1. A.R. Harvey, J. Beale, A.H. Greenaway, T.J. Hanlon and J. Williams, "Technology options for imaging spectrometry" in *Imaging Spectrometry VI*, Descour & Shen, Proc. SPIE **4132**, 13-24 (2000).
2. P.J. Miller and A.R. Harvey, "Signal to noise analysis of various imaging systems" in *Biomarkers and Biological Spectral Imaging*, Bearman, Bornhop & Levenson, Proc. SPIE **4259**, 16-21 (2001).
3. S.P.Davis, M.C.Abrams and J.W.Brault, *Fourier Transform Spectrometry* (Academic Press, 2001).
4. M.J.Persky, "A review of space infrared Fourier transform spectrometers for remote sensing," Rev. Sci. Instrum. **66**, 4763-4797 (1995).
5. A.R. Harvey and D.W. Fletcher-Holmes, "Imaging Apparatus," Patent WO2004 005870 A1, (2004).
6. J W Brault, "New approach to high-precision Fourier-transform spectrometer design," Appl. Opt. 35, pp2891-2896 (1996)
7. G. Zahn, K. Oka, T. Ishigaki and N. Baba, "Birefringent imaging spectrometer," Appl. Opt. **41**, 734-738 (2002).
8. R. Heintzmann, K.A. Lidke and T.M. Jovin, "Double-pass Fourier transform imaging spectroscopy," Optics Express, **12**, pp 753-763 (2004)
9. L. J. Otten, A. D. Meigs, B. A. Jones, P. Prinzing, and D. S. Fronterhouse, "Payload Qualification and Optical Performance Test Results for the MightySat II.1 Hyperspectral Imager," Proc. SPIE. **3498**, pp. 231-238 (1998)
10. J. Genest, P. Tremblay, and A. Villemaire, "Throughput of tilted interferometers," App. Opt. **37**,21, pp. 4819-4822. 1998
11. M. Hashimoto and S. Kawata, "Multichannel Fourier-transform infrared spectrometer," Appl. Opt. **31**, 6096-6101 (1992).
12. M.J. Padgett and A.R. Harvey, "A static Fourier-transform spectrometer based on Wollaston prisms," Rev. Sci. Instrum. **66**, 2807-2811 (1995)
13. A.R.Harvey, "Determination of the optical constants of thin films in the visible by dispersive Fourier transform spectroscopy," Rev. of Sci. Instr.69, pp3649-3658 (1998)
14. S. Prunet, B. Journet and G. Fortunato, "Exact calculation of the optical path difference and description of a new birefringent interferometer," Opt. Eng. **38**, 983-990 (1999).

#5084 - $15.00 US Received 19 August 2004; revised 19 October 2004; accepted 19 October 2004

15. R.F. Horton, "Optical design for a High Etendue Imaging Fourier Transform Spectrometer" in *Imaging Spectrometry II*, Descour & Mooney, Proc. SPIE **2819**, 300-315 (1996).
16. M. Françon and S. Mallick, *Polarization Interferometers Applications in Microscopy and Macroscopy* (Wiley-Interscience, 1972).
17. Labview virtual instrumentation software for personal computers, (National Instruments, 2003), http://www.ni.com/labview/ .
18. Labsphere Inc, 231 Shaker Street, POB 70, North Sutton, NH 03260, USA.

## 1. Introduction

It is widely appreciated that Fourier-transform spectrometry offers important advantages over other techniques. Prominent among these is the high signal-to-noise ratio that accrues from the Fellget multiplex advantage and the Jacquinot étendu advantage, although, the former of these is valid only for the low-light, shot-noise-limited conditions commonly found in, for example, mid-infrared applications [1,2]. Other important advantages are the wide free-spectral-range and high spectral resolutions that are possible. For detailed discussion of Fourier-transform spectrometry see references [3,4]. It is natural therefore that Fourier-transform spectrometry has been developed for two-dimensional spectral imaging in which the spectra for all pixels within a two-dimensional scene are recorded in parallel to form a spectral image cube of the scene [1].

Traditional Fourier-transform spectrometers are based on mechanically scanned mirrors; the stability and precision requirements for these instruments mean that their use in hostile environments requires significant sophistication in construction [4]. In this paper we present a new technique in Fourier-transform hyperspectral imaging that is inherently robust and offers a greatly reduced need for complexity in design and construction for such applications [5]. A conventional Fourier-transform imaging spectrometer (FTIS) employs a mechanically scanned Michelson interferometer in the pupil-plane of a conventional imager. Scanning one of the mirrors of the interferometer varies the optical path difference between the two arms of the interferometer to produce an interferogram at each pixel in the detector array as a function of a temporally scanned path difference. Fourier transformation of the interferograms yields the spectrum of the light at each pixel, enabling a spectral data cube to be generated from the recorded interferogram cube.

There are two major difficulties in applying this technique outside of the controlled conditions of an optical laboratory:

- The mirror movement is required to scan the moving mirror with an accuracy and precision of better than $\lambda/20$ (that is, better than 20 nm for blue light). This is difficult to achieve in the laboratory without sophisticated, high-cost mechanical components and servo-controlled movements or additional laser interferometers and associated signal processing [6]; in harsh environments obtaining the required performance is a major challenge.
- Small physical disturbances of the interferometer introduce phase-noise into the path differences between the two arms that washes out the interferogram,

Reduced sensitivity to vibration and increased robustness have been demonstrated in imaging [7-10], and single-pixel [11-15] FT spectrometry, employing static interferometers that produce spatial interferograms. The use of a slit that needs to be scanned to produce a two-dimensional image means that the full optical throughput advantage (that is, the Fellget multiplex advantage) of two-dimensional FT imaging spectrometry is not obtained and the signal-to-noise ratios obtained are no higher than for conventional dispersive hyperspectral imagers that also employ a slit [1], whilst they nevertheless suffer from the problems afflicting Fourier-transform spectrometers, namely; the bias on the interferogram can lead to detector saturation, the number of data points recorded is significantly larger than the number of useful data points in the calculated spectra and random access to specific spectral bands with

#5084 - $15.00 US Received 19 August 2004; revised 19 October 2004; accepted 19 October 2004

optimized integration times is not possible. Furthermore, the maximum spectral resolution is limited for this type of FT spectrometer by the detector pixel count.

The FTIS described here is based on a novel scanning birefringent interferometer that enables two-dimensional spectral imaging without spatial scanning and that retains the traditional advantages of Fourier-transform spectral imaging, as described above, but is inherently robust and insensitive to vibration. The precision and accuracy required of the optical components can be typically two orders of magnitude lower than is required of a traditional instrument. The spectral range of such instruments is limited only by the availability of transmissive, birefringent materials and detector sensitivity; we have identified materials that enable operation in wavebands between 200 nm and 14μm.

The principle of the technique is described in Section 2, results from proof-of-principle experiments are presented in Section 3 with discussion and conclusions in Section 4.

## 2. Fourier-transform imaging spectrometer technique

### *2.1. Principle of operation*

The birefringent interferometer used in the birefringent FTIS [5,12-14] is shown in Fig. 1. It consists of two Wollaston prisms (WP) of equal and opposite splitting angles located close to the exit pupil of a conventional imaging configuration. Light from the scene is resolved by polarizer 1 into linearly polarized light at 45° to the optic axes of the Wollaston prisms. The transmitted light is resolved by the first WP into two equal amplitude, orthogonally polarized components that diverge slightly. Transmission through the second WP refracts the two components so that they propagate collinearly and are focused by the imaging lens to a common location at the detector array where they interfere. This apparatus constitutes a polarizing interferometer, which enables a path difference to be introduced between the orthogonally polarized components. For light from a specific point in the scene, this path difference is uniform across the width of the aperture and is modulated by translation of the second Wollaston prism, as described below.

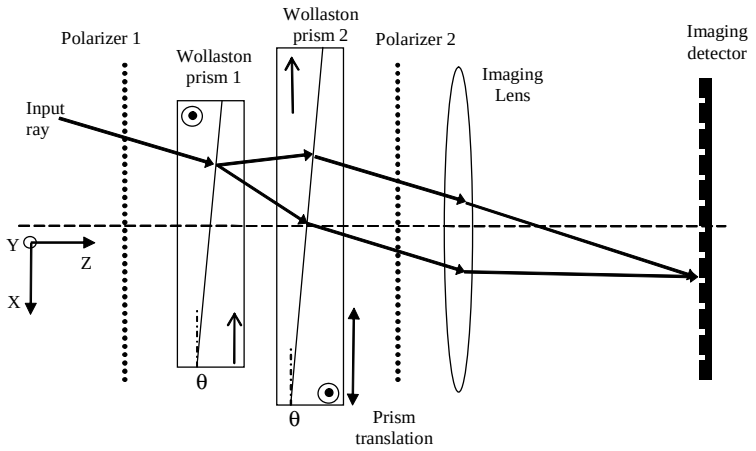


Fig. 1. A schematic of the birefringent polarizing interferometer employed by the Fourier-transform hyperspectral imager. The optic axes within the Wollaston prisms are indicated by arrows and circles.

For simplicity, we consider initially only light incident normally to the input surface of the first Wollaston prism. The path difference introduced by a Wollaston prism between orthogonal polarization states of a normally incident ray with a small splitting angle is given by the approximation [16]

$$\Delta_{\mathrm{OPL}} \approx 2db\tan\theta\,, \tag{1}$$

#5084 - $15.00 US Received 19 August 2004; revised 19 October 2004; accepted 19 October 2004

where $d$ is the displacement of the ray from the centerline of the prism, $b=(n_o-n_e)$ is the birefringence of the Wollaston prism material where $n_o$ and $n_e$ are the ordinary and extraordinary refractive indices and $\theta$ is the prism wedge angle. The path difference for consecutive transmission through two Wollaston prisms with equal splitting angles, with the optic axes aligned as shown in Fig. 1, can be easily shown to be

$$\Delta_{\mathrm{OPL}} = 2bh\tan\theta \tag{2}$$

where $h$ is the offset of the centers of the two Wollaston prisms.

The output rays are resolved into a common polarization state by the output polarizer, and brought to a focus on the detector where they interfere with a mutual path difference, $\Delta_{\mathrm{OPL}}$. Translation of the second Wollaston prism so as to vary $h$ introduces a time varying path difference between the two components, enabling an interferogram to be recorded as a function of prism displacement. Whereas the mirror in a Michelson interferometer is scanned along the optical axis, here the Wollaston prism is scanned transversely to produce the temporal interferogram.

For a specific field angle, the optical path difference is uniform across the width of the Wollaston prisms, but varies slowly with the angle that the ray makes with the optical axis. For a fixed displacement of the Wollaston prisms, this results in a hyperbolic fringe pattern at the detector [16] which corresponds to an unimportant hyperbolic variation, across the detector array, in the zero-path-difference of the interferogram recorded at each pixel.

*2.2. The Fourier-transform relationship*

The formal derivation of the Fourier transform relationship starts by calculating the complex amplitudes of the interfering fields. If $\tau_1$ and $\tau_2$ are amplitude transmittances of the two polarisers, then the amplitude of the optical field at a particular pixel at an optical angular frequency $\omega$, in a small interval of optical frequencies d$\omega$, and at a prism displacement, $h$, is given by

$$\varepsilon_T(\omega,h)\mathrm{d}\omega = \tau_1\tau_2\varepsilon_o(\omega)\left[\exp\left(\mathrm{i}\omega\left(t+hb\tan\theta/c\right)\right)\pm\exp\left(\mathrm{i}\omega\left(t-hb\tan\theta/c\right)\right)\right]\mathrm{d}\omega, \tag{3}$$

where $\varepsilon_o(\omega)$ is the amplitude of the light incident upon the first polarizer, $t$ is time and $c$ is the speed of light. The sign of the second term is positive if the polarisers are co-aligned and negative if they are crossed. The intensity of the recombined beams is then

$$I(\omega,h)d\omega = 2\varepsilon_o{}^2(\omega)\left|\tau_1\tau_2\right|^2\left[1\pm\cos\left(2\omega bh\tan\vartheta/c\right)\right]d\omega. \tag{4}$$

Integrating the total flux at displacement $h$ for all frequencies yields:

$$I(h) = 2\left|\tau_1\tau_2\right|^2\left(I_o\pm\int_0^\infty I_o(\omega)\cos\left(2\omega bh\tan\theta/c\right)d\omega\right) \tag{5}$$

where $I_o$ is a bias term and $I(\omega)=\varepsilon_o(\omega)^2$ is the spectral intensity at frequency ω. The second term in equation 5 is the interferogram which is the Fourier cosine transform of the spectrum with $2b\tan\theta$ acting as the constant of proportionality with respect to the length variable $h$. Inverse Fourier transformation of the interferogram yields $I(\omega)$.

The interferogram is sampled with a sampling interval $\Delta_h$ of the Wollaston prism such that the Nyquist criterion for the short-wavelength cutoff of the system spectral response is obeyed. Discrete inverse Fourier transformation of the sampled interferogram yields the spectral distribution, which is sampled at the values:

#5084 - $15.00 US Received 19 August 2004; revised 19 October 2004; accepted 19 October 2004

$$\sigma_i = i \frac{1}{2b(\sigma_i) N \Delta_h \tan\theta}, \tag{6}$$

where $\sigma = \omega / 2\pi = 1/\lambda$, $N$ is the number of samples in the interferogram and $i$ ranges from 0 to $N/2$. Given appropriate functional forms of $b(\sigma_i)$ equation 6 can be solved for $\sigma_i$.

*2.3. Advantages of this technique*

The constant of proportionality, $2b\tan\theta$, in equations (4-5) can be considered as an optical gearing ratio, $G$, of the system; that is to say, a displacement $h$ of the Wollaston prism introduces an optical path difference $hG$. The value of $G$ is a design parameter, but is typically less than $10^{-2}$, whereas for a Michelson interferometer, $G$=2. This small value of $G$ for a birefringent interferometer greatly reduces the refinement required of the moving parts. Firstly, the required accuracy of the scanning mechanism is reduced from, λ/20 for a Michelson interferometer, to λ/(10G) (typically about 10λ) for a birefringent interferometer; a greater than 200-fold reduction. The sensitivity to vibration in the direction of movement of the Wollaston prism is also reduced by the same factor in comparison to the sensitivity to vibration of a Michelson interferometer. For vibrations in other directions, and for air currents, the near-collinear propagation of the interfering beams means that these disturbances are common mode and have negligible effect. This contrasts strongly with Michelson interferometers that require enclosed and isolated instruments to ensure adequate performance.

It is important to note that these improvements in robustness are attained with only a modest compromise in optical efficiency: an ideal Michelson interferometer is 50% optically efficient, since half the light is reflected back towards the source, whilst the ideal birefringent interferometer is 50% efficient in polarized light and 25% efficient in unpolarized light. The use of polarizing beam splitters in place of film polarizers would enable multiple detectors to be used; increasing optical efficiency to 50% in unpolarized light and 100% in polarized light. The Jaquinot advantage is also retained in principle [13], but since the pixels used in FTIS detectors are normally much smaller than a spatial fringe for all but very high resolving powers, this is not exploited.

The wide free spectral range is an important advantage of Fourier-transform spectrometry. We have identified a range of birefringent materials that enable operation between wavelengths of 200 nm and 14 μm. In practice the spectral range will be limited by the detector used; with its large birefringence, calcite enables compact Wollaston prisms to be used across the spectral range from 370-2,300 nm covered by, for example, silicon and InGaAs detectors; quartz and magnesium fluoride enable coverage in the ultraviolet and visible, although their lower birefringences mean that the Wollaston prisms will be larger; for infrared wavelengths between about 2 and 14 μm cadmium selenide and cadmium sulfide are suitable birefringent materials although at least two different detectors based on, for example, InSb or cadmium mercury selenide technology, would be required to cover this range.

## 3. Experiment and results

A birefringent Fourier transform imaging spectrometer was constructed according to the scheme in Fig. 1 using calcite ($n_o$-$n_e$≈0.175) Wollaston prisms with a wedge angle of 1.5°. The prism dimensions were such that $N\Delta_h$ was limited to a maximum value of 10 mm giving a limiting spectral resolution of 110 $cm^{-1}$. The second Wollaston prism was mounted on a motorized translation stage; computer control of the stage motion, image acquisition and all data processing was accomplished with *Labview* software [17].

Images are presented here for which the light source was a tungsten filament lamp, and the detector is a CCD array, yielding a spectral range of about 10,000-25,000 $cm^{-1}$ (1000-400 nm). An example image, taken from the included movie file, of five spectral calibration tiles [18] imaged through the interferometer is shown in Fig. 2(a). The hyperbolic fringes arise from the variation of path difference with field angle as was described in Section 2.1. As can

#5084 - $15.00 US Received 19 August 2004; revised 19 October 2004; accepted 19 October 2004

be seen from the movie, temporal scanning of the mirror produces a time-sequential interferogram at each pixel, as a function of Wollaston prism displacement; an example interferogram is shown in Fig. 2(b). Note that the horizontal scale, in mm, is the displacement of the Wollaston prism; the equivalent displacement of the mirror in a Michelson interferometer would be some 200-fold smaller. Inverse Fourier transformation of the complete data cube of interferograms produces a spectrum for each pixel; that is, the spectral data cube. An example narrow-band image of the calibration tiles calculated from the spectral data cube and normalized to give albedo is shown in Fig. 2(c). The associated movie file shows the complete spectral data cube as an animation. The spectral albedo data cube of two plants appears as a movie file in Fig. 2(d). Several features are readily apparent; in particular, the distressed leaf of the plant on the right exhibits high contrast with the healthy leaves from the same plant for optical frequencies close to 16,000 $cm^{-1}$ and the so-called chlorophyll edge is very noticeable as a rapid increase in albedo close to 14,000 $cm^{-1}$.

It is apparent in these animations that the SNR of the data is low at the extremes of wavenumber, where the camera response and source spectrum combine to produce little measurable signal. Whereas, for spectrometry based on monochromation, the spectral range can be restricted to yield data that always has a high SNR, it is a fundamental feature of Fourier-transform spectrometry that spectra with a wavenumber smaller than the low-wavenumber cutoff of the detector is generated, even though it is essentially pure noise, and Nyquist sampling of the interferogram requires that the signal is reduced to the noise floor at the high wavenumber limit.

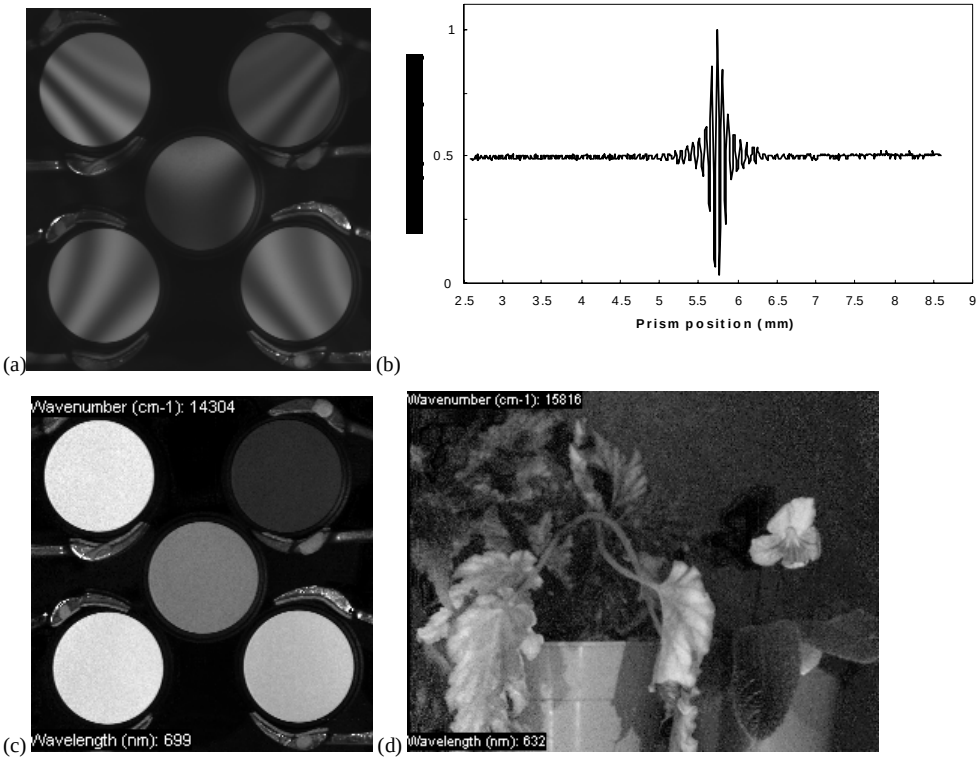


Fig. 2. (a) An image of an extended scene consisting of 5 spectral calibration tiles; the associated animation file has a size of 1.5 Mb, (b) an example interferogram recorded at one of the pixels as a function of displacement of the Wollaston prism, (c) absolute albedo image; the associated animation file has a size of 1Mb and (d) albedo image of house plants; the associated animation file has a size of 1.1Mb.

#5084 - $15.00 US Received 19 August 2004; revised 19 October 2004; accepted 19 October 2004

In movie sequences for Figs. 2(a) and 2(c) it is noticeable that for the images at the high-frequency end of the spectrum and with low signal-to-noise ratios, hyperbolic fringe artifacts appear across the images. Analysis indicates that these artifacts are probably caused by certain combinations of interfering rays reflected from the surfaces of the Wollaston prisms incurring a treble pass and a doubling of the effective path difference introduced. Relatively intense, direct light at a wavelength $\lambda$ therefore produces an interferogram that interferes with the interferogram caused by less intense light of wavelength $\lambda/2$ to produce increased and decreased intensity at certain directions. The hyperbolic form of the interferograms is believed to be due to the hyperbolic variation of the added path difference caused by the second and third passes through the Wollaston prisms. The Wollaston prisms used were not anti-reflection (AR) coated and it is expected that AR coating will significantly suppress this artifact.

## 5. Conclusions

We have demonstrated a new type of Fourier-transform imaging spectrometer, which, through its inherent robustness and compactness, promises to enable the recognized benefits of Fourier-transform imaging spectrometry to be obtained in harsh environments, such as for airborne remote sensing and industrial inspection, for the first time.

This technique may be applied at all wavelengths for which detectors and birefringent materials are available; this enables operation between 200 nm and 14 μm. The high SNR at low fluxes is particularly beneficial for low-light imaging in the visible and also in the 3 to 5 μm band where photon fluxes are low and detector saturation is less problematic [1].

## Acknowledgments

This work was carried out with funding from Sensors and Electronic Warfare Research Domain of the UK MoD Corporate Research Programme.

#5084 - $15.00 US Received 19 August 2004; revised 19 October 2004; accepted 19 October 2004